JOURNAL OF GEOPHYSICAL RESEARCH, VOL. 104, NO. C4, PAGES 7625–7639, APRIL 15, 1999

Coupled sea surface–atmosphere model 2. Spectrum of short wind waves

V. N. Kudryavtsev

Marine Hydrophysical Institute, Sevastopol, Ukraine

V. K. Makin

Royal Netherlands Meteorological Institute, De Bilt, Netherlands

B. Chapron

Institut Français de Recherche pour l'Exploitation de la Mer, Plouzané, France

Abstract. A physical model of the short wind wave spectrum in the wavelength range from a few millimeters to few meters is proposed. The spectrum shape results from the solution of the energy spectral density balance equation. Special attention is paid to the description of the capillary range of the short wave spectrum. It is assumed that in this range the spectrum shape is determined mainly by the mechanism of generation of parasitic capillaries. This is described as the cascade energy transfer from the gravity to the capillary waves. Thus the capillary wave spectrum results through the balance between generation of capillaries and their viscous dissipation. The short gravity wave spectrum results through the balance between wind input and dissipation due to wave breaking. A paramctcrization of wind input is obtained in part 1 of the present paper. To describe the dissipation due to wave breaking, the approach developed by *Phillips* [1985] is used. The spectral rate of energy dissipation is presented in the form of a power dependence of the ratio of the saturation spectrum to some threshold level. It is further shown that the threshold level depends on the drift current shift in the water viscous sublayer, which affects the energy losses by wave breaking. To obtain a short wave spectrum which is valid in the whole wavenumber domain, the capillary and the short gravity wave spectra are patched in the vicinity of the wavenumber corresponding to the minimum phase velocity. This short wave spectrum is incorporated into the wind over waves coupled model developed in part 1 of the present paper. The measured statistical properties of the sea surface related to the short waves, such as the spectral shape of omnidirectional and up-wind spectra, their wind speed dependence and angular spreading, and the wind speed dependence of integral mean square slope and skewness parameters, are well reproduced by the model. Also the model well reproduces the measured wind speed dependence of the drag coefficient and of the coupling parameter.

1. Introduction

Wind over waves coupled models [e.g., *Janssen*, 1989; *Makin et al.*, 1995; *Makin and Kudryavtsev*, this issue] have shown that short gravity and capillary-gravity waves support a significant fraction of the total momentum flux to the sea surface. A reliable description of the short wave spectrum is thus of crucial importance to better determine the exchange of momentum, heat, and gases between the ocean and the atmosphere. Short gravity and capillary-gravity waves also serve as roughness elements on the ocean surface to scatter electromagnetic waves. Therefore the practical application of radar instruments for ocean remote sensing brings further the demand for wavenumber spectral models in the short gravity and capillary-gravity range.

Recently, empirical models of the short wave spectrum have been developed [e.g., *Apel*, 1994; *Elfouhaily et al.*, 1997], which are based on the functional approximation of measurements. For instance, Apel paid special attention to the correct description of the capillary-gravity range of the wave spectrum as reported by *Jähne and Riemer* [1990] in their laboratory experiments, while *Elfouhaily et al.* [1997] explicitly con-

Paper number 1999JC900005.
0148-0227/99/1999JC900005$09.00

strained their spectrum to conform to *Cox and Munk*'s [1954] slick and clean surface slope measurements.

To further gain understanding and, for example, to better interpret high-resolution radar image contrasts from synthetic aperture radar instruments, a physical model of the short gravity and capillary-gravity wave spectrum is more appropriate, as it will potentially describe the physical properties of the sea surface under the joint action of wind and surface currents of arbitrary origin. Such a model is based on the solution of the energy spectral density balance equation which describes the growth, evolution, and decay of waves due to different physical processes.

Assuming that wind input, wave-wave interactions, and dissipation due to wave breaking are proportional to each other in the gravity range of the wave spectrum, *Phillips* [1985] obtained a wave variance spectrum F of the form $F(k) \sim (u_*/c)k^{-4}$ (here u_* is the friction velocity of the air, k is the wavenumber, and c is the phase speed), which agrees well with measurements made by *Toba* [1973]. A similar spectral shape was derived by *Zakharov and Zaslavskii* [1982] and *Kitaigorodskii* [1983] on the basis of a rather different assumption: namely, that in the equilibrium range the energy input from the wind occurs primarily at the energy-containing scales while dissipation is restricted to much shorter scales. *Donelan and Pierson* [1987] suggested that in the short gravity and capillary range wave-wave interactions can be neglected, and the wave spectrum results from a balance between wind input and energy dissipation due to small-scale breaking and viscosity. However, such a spectrum underestimates the energy level of the capillary waves as compared to experiments by, for example, *Jähne and Riemer* [1990].

Recently, *Belcher and Vassilicos* [1997] followed a new approach to develop a model of the equilibrium range of gravity waves. Their approach is based on kinematical and dynamical properties of breaking waves. It is assumed that wave spectra are dominated by the singularities in slope of self-similar breaking crests. The shape of the wavenumber spectrum of gravity waves is shown to vary as $\sim k^{-4}$, which is in a good agreement with recent data. Here in part 2 of the present paper we shall follow an approach based on the energy spectral density balance equation to construct a physical model of the short wind wave spectrum in the range of wavelengths from a few millimeters to a few meters.

The main innovation of the model is the description of the wave spectrum in the capillary range, which follows *Kudryavtsev* [1996]. The general idea is that capillary waves are generated on the crests of steep short gravity waves as they break, while the wind input plays no significant role in the generation of capillaries. The generation of "parasitic" capillaries was first studied theoretically by *Longuet-Higgins* [1963] and experimentally by *Cox* [1958]. In the present paper the generation of parasitic capillaries is described in terms of the spectral nonlinear cascade energy flux from the gravity spectral interval into the capillary interval. This cascade energy flux provides the loss of energy of the short gravity waves, and the supply of energy to the capillary waves. The energy of capillary waves in turn dissipates due to the action of molecular viscosity. The balance between cascade generation and viscous dissipation defines the spectral form in the capillary range $k > (g/\gamma)^{1/2}$, where g is the acceleration of gravity, and γ is the kinematic surface tension of water. In the capillary-gravity range $k \sim (g/\gamma)^{1/2}$ a balance between wind input, viscous dissipation, and resonant three-wave interactions determines the spectral form.

In the short gravity range the spectral form results through a balance between wind input and dissipation due to small-scale breaking (including generation of parasitic capillaries). The wind input term is described in part 1 of the present paper. We follow *Phillips* [1985] to describe dissipation due to breaking: the spectral energy dissipation is related to the density of frequency of wave breaking events. We then assume this density depends on the ratio of the saturation spectrum to some threshold level. We show that this threshold level in turn depends on the shear of the drift current in the water molecular sublayer. This is an important new element in the parameterization of dissipation due to breaking, as it accounts for dissipation of small-scale waves on the drift current, which, as we will show, could be significant.

The three spectral forms, resulting from a different balance in the equation of the energy spectral density, can be described by the generalized model of the short wave spectrum proposed in the paper. This model is included in the wind over waves coupling scheme developed in part 1 of the paper. The coupled sea surface–atmosphere model gives a self-consistent description of short waves and the atmospheric boundary layer. The energy level of short waves is determined to a large extent by wind input, which is determined in turn by the spectral form of the wave spectrum. The coupling of a physical model of short waves to the atmosphere is viewed as a principle result of the present paper. In potential, the coupled system gives the possibility to directly relate any change in the energy level of short waves to the air-sea momentum exchange (the sea drag) and thus to the surface wind.

The shape of the short wave spectrum and its integral characteristics (mean square slope and skewness) are compared to available field and laboratory measurements, and a reasonable agreement is found. Consistency in the interaction between wind and waves (momentum flux to the surface, drag coefficient, coupling parameter) is shown as well.

2. Terms of the Short Waves Energy Balance

The physical model of the short wind wave spectrum results from the equation of the energy spectral density balance which has the form [e.g., *Phillips*, 1977, 1985]

$$\frac{D}{Dt}E(\vec{k},\vec{x},t) + S_{ij}\frac{\partial u_i}{\partial x_j} = Q, \tag{1}$$

where E is the energy spectral density, the total derivative is taken along a wave ray in $(\vec{k},\vec{x})$ space, S_{ij} is the radiation stress tensor, u_i is the surface current component, and Q is the energy source term. The energy spectrum is related to the wave variance spectrum $F(\vec{k},\vec{x},t)$, which characterizes the statistical properties of the sea surface, by the relation

$$E(\vec{k},\vec{x},t) = \frac{\omega^2}{k}F(\vec{k},\vec{x},t), \tag{2}$$

where the wave frequency ω and the wavenumber k satisfy the dispersion relation

$$\omega^2 = gk + \gamma k^3. \tag{3}$$

The source term Q is written in the form

$$Q = \frac{\rho_a}{\rho_w}\beta\omega E - 4\nu k^2 E - \mathcal{D} + P - \nabla\cdot\vec{T}. \tag{4}$$

The first term on the right-hand side is the wind input written in terms of the growth rate parameter β; the second term describes the energy loss due to viscous dissipation (ν is the kinematic viscosity of water); $\mathcal{D}$ is dissipation due to wave breaking and generation of parasitic capillary waves; P is the source of nonlinear cascade generation of capillary waves by steep short gravity waves; $\nabla\cdot\vec{T}(\vec{k})$ represents the net spectral flux of energy through the wavenumber k by resonant wave-wave interactions. To find the shape of the short wind wave spectrum, we need an explicit relation for each term in the equation of the energy spectral density balance.

2.1. Wind Input

The parameterization of the growth rate parameter β is discussed in details in part 1 of this paper [*Makin and Kudryavtsev*, this issue]. The fact that the turbulent stress is not constant with the height above waves dictates the following expression for the growth rate parameter

$$\beta(k,\theta) = c_\beta\left[1-\alpha_c\bar{f}(k)\right]\left(\frac{u_*}{c}\right)^2\cos\theta|\cos\theta|, \tag{5}$$

where θ is an angle between the wind and the wavenumber vector; α_c is the coupling parameter defined as the ratio of the wave-induced stress at the surface (the form drag) and the total stress u_*^2 (equation (7) in part 1); $\bar{f}(k)$ is the averaged dimensionless wave-induced stress (equation (29) in part 1) related to a k component; $c_\beta = m_\beta R$ where m_β is a constant, and R is a relaxation function which accounts for the fact that the growth rate of fast moving waves tends to zero (relation (31) in part 1). In part 1 we show that $m_\beta = 0.045$. For short waves $c_\beta = m_\beta$, $\bar{f}(k)\to 1$ and (5) reduces to

$$\beta(k,\theta) = m_\beta\left[1-\alpha_c\right]\left(\frac{u_*}{c}\right)^2\cos\theta|\cos\theta|. \tag{6}$$

Relation (6) differs from the parameterization of *Plant* [1982] by a factor $(1-\alpha_c)$. The parameterization of β via the surface stress $(1-\alpha_c)u_*^2$ can be explained by the sheltering theory of wave growth [*Belcher and Hunt*, 1993], where the energy flux to waves results from the dynamics of the turbulent stresses in a very thin layer adjacent to the wave surface.

2.2. Generation of Parasitic Capillary Waves

When short gravity waves (SGW) (in the wavelength range 0.03-0.3 m) approach their maximum steepness, they generate parasitic capillary waves (CW) on their forward face [*Longuet-Higgins*, 1963; *Crapper*, 1970; *Ruvinsky et al.*, 1991]. These capillaries are well observed in laboratory experiments [e.g., *Chang et al.*, 1978; *Yermakov et al.*, 1986]. They are generated in the vicinity of SGW crests when the curvature of SGW attains large values. As the group velocity of the CWs exceeds their phase velocity, they travel along the forward face of the SGW and disappear due to the molecular viscosity.

2.2.1. Governing equations. Relative to SGWs, parasitic CWs are stationary, and their apparent frequency equals zero

$$\omega + kU = 0, \tag{7}$$

where ω and k are the intrinsic frequency and the wavenumber of the capillary wave satisfying dispersion relation (3); U is the surface current velocity in a coordinate system moving with the phase velocity C of the SGW,

$$U(x) = u(x) - C, \tag{8}$$

and $u(x)$ is the orbital velocity of the SGW. As $u/C \ll 1$ everywhere except at the crest, where the CWs are generated, we neglect u in (8). From (7) and the dispersion relationship (3) follows the relation between the SGW (K) and the CW (k) wavenumber

$$k = \frac{g}{\gamma K}. \tag{9}$$

Parasitic capillaries extract energy from short gravity waves which leads to the attenuation of the latter. Let us assume that at some moment an energy source supporting the existence of the steep SGW carrying parasitic capillaries is "switched off". Then the total energy of the system SGW-CW will change as

$$\frac{\partial}{\partial t}\left(e_g + e_c\right) = -4\nu k^2 e_c - 4\nu K^2 e_g \tag{10}$$

where e_g is the SGW energy, and e_c is the CW energy. Equation (10) shows that the total energy can change only due to viscous dissipation. It can be shown that if a SGW and a CW have the same steepness, the ratio of e_c and e_g, as well as the ratio of SGW's and CW's viscous dissipation rates, have an order of $K/k = g/(\gamma k^2) \ll 1$. Equation (10) can be written then as

$$\frac{\partial}{\partial t}e_g = -4\nu k^2 e_c. \tag{11}$$

This equation has a clear physical sense. It shows that the nonlinear cascade losses of the SGW energy, caused by parasitic CWs, are equal to the CW energy losses due to molecular viscosity. The nonlinear dissipation of the SGW energy D is thus

$$D(K) = -4\nu k^2 e_c(k), \tag{12}$$

where the wavenumber of the SGW K and the wavenumber of the CW k are related through (9).

Equation (12) describes the energy dissipation of one "individual" SGW. If we assume that the sea surface is a superposition of a narrowband random SGWs, the rate of SGW energy dissipation due to the sporadic generation of parasitic CWs is a random function of space and time. In this case, the relationship between the averaged SGW dissipation D and the averaged CW energy e_c is again defined by (12), where the average is taken over an ensemble of individual SGWs emitting CWs.

2.2.2. Spectral source of parasitic capillaries. Equation (12) may now be considered as the balance equation of the CW energy. It shows that the cascade energy flux $D(K)$ from the SGW spectral domain $KdKd\theta$ is balanced by the viscous dissipation of the CW energy, which is concentrated in the spectral domain $kdkd\phi$. This energy flux results in dissipation of SGW energy. With a definition of the spectral density of the CW energy as $e_c = E(k,\phi)kdkd\phi$, and with a definition of the spectrum of the SGW energy dissipation due to the nonlinear cascade generation of CWs as $D = \mathcal{D}(K,\theta)KdKd\theta$, (12) becomes

$$4\nu k^2 E(k,\phi) = P(k,\phi), \tag{13}$$

where

$$P(k,\phi) = \mathcal{D}(K,\theta)\frac{KdKd\theta}{kdkd\phi}. \tag{14}$$

Experimental studies [e.g., *Yermakov et al.*, 1986; *Zhang*, 1995] show that a train of parasitic capillaries is parallel to a crest of a short gravity wave which generates them. Hence a band of SGWs propagating in the range $d\theta$, generates a train of CWs within the same range of directions, that is, $d\phi = d\theta$. With (9) we have

$$\frac{KdKd\theta}{kdkd\phi} = \left(\frac{k_c}{k}\right)^4, \tag{15}$$

where $k_c = (g/\gamma)^{1/2}$ is the wavenumber corresponding to the minimum of the phase speed. The source of parasitic CWs in the balance equation (13) takes the form

$$P(k,\theta) = \left(\frac{k_c}{k}\right)^4 \mathcal{D}(K,\theta), \tag{16}$$

where from (9) $K = k_c^2/k$. Equation (16) gives an explicit expression for the nonlinear cascade source term P in (4).

Equation (16) is not valid at very high wavenumbers. Indeed, parasitic capillaries can not be effectively generated by all gravity waves. *Yermakov et al.* [1986] report that even under laboratory conditions they could not observe trains of parasitic CWs on SGWs longer than 30 cm. In real conditions, the crests of the decimeter gravity waves break rather than generate trains of capillaries. Hence if we assume that SGWs with wavelengths longer than 10-15 cm do not generate CWs, but break and lose their energy to generate turbulence, then the applicability of (16) is restricted to the wavenumber range $k < 2000 - 3000$ rad m^{-1}.

2.2.3. Estimate of the capillary wave spectrum. From (13) and (16) we can estimate the shape of the capillary spectrum. In the capillary range the energy input from the wind does not play a dominant role. The growth rates of parasitic CWs and their associated SGWs are equal, since their phase speeds are equal. Therefore the ratio of the wind input to the CWs and the source term P is

$$\left(\frac{k_c}{k}\right)^2 \frac{B(k,\theta)}{B(K,\theta)} \ll 1, \tag{17}$$

where $B = k^4 F$ is the saturation spectrum. If the SGWs are in an equilibrium state, their dissipation due to the generation of parasitic capillaries is equal or proportional (if resonant wave-wave interactions are important) to their energy input from the wind, that is,

$$\mathcal{D}(K,\theta) \sim \beta g^{-3/2} K^{-7/2} B(K,\theta). \tag{18}$$

The relationship between the saturation spectra $B(k,\theta)$ and $B(K,\theta)$ follows from (13), (16), (18), and (6),

$$B(k,\theta) \sim \frac{(1-\alpha_c)u_*^2}{\nu\gamma^{1/2}k^{3/2}} B(K,\theta)\cos\theta|\cos\theta|. \tag{19}$$

From (19) it follows that the CW spectrum is strongly wind dependent, decreases with increasing wavenumber, and its angular spreading is narrower than the SGW one. This is qualitatively consistent with the form of the measured capillary spectra reported by *Jähne and Riemer* [1990] and *Zhang* [1995].

To obtain an explicit estimate of the CW spectrum, the upwind saturation spectrum of short gravity waves is specified as $B(K,0) \sim (u_*/c)$ [*Toba*, 1973; *Phillips*, 1985]. In this case the CW spectrum (19) is

$$B(k,0) \sim (1-\alpha_c)u_*^3 \nu^{-1}\gamma^{-1}k^{-2}. \tag{20}$$

The wind speed dependence of the model spectrum (20) is cubic which is in close agreement with the $u_*^{2.5}$ dependence reported by *Jähne and Riemer* [1990]. The k^{-2} wavenumber dependence is also consistent with measurements of *Jähne and Riemer* [1990] and *Zhang* [1995].

2.3. Energy Dissipation Due to Wave Breaking

Wave breaking is a rather rare event on the sea surface. Hence wave breaking is a local process in physical

space but is a distributed process in Fourier space. An experimental study of the energy loss of an individual wave breaker was done by *Duncan* [1981]. The shape of breakers was found to be geometrically similar for waves of different scales. The rate of energy loss D per unit surface in a breaker moving with the phase speed c was found to be

$$D = bc^3, \tag{21}$$

where b is an empirical constant of order 0.01. The wavenumber of the wave carrying a breaker is identified by its phase speed $k = (g/c)^{1/2}$.

Following *Phillips* [1985], we consider the density of frequency of wave breaking events $N(\vec{c})$ passing a given point at the surface with velocities of advance between $\vec{c}$ and $\vec{c} + d\vec{c}$. The expected number of breakers passing a given point per unit time is then $N(\vec{c})d\vec{c}$. With (21) the average rate of the energy dissipation of waves by breakers with velocities in the range $\vec{c}$ to $\vec{c} + d\vec{c}$ can be written as

$$D = 2\pi b g^{-1} c^4 N(\vec{c}) d\vec{c}. \tag{22}$$

When every wave crest in the wave field breaks, the quantity $2\pi g^{-1} c N(\vec{c}) d\vec{c}$ is close to 1 and (22) reduces to (21). At sea, however, the fraction of wave crests carrying a breaker is small. This means that although the energy of a breaking wave is concentrated in a small area $d\vec{k}d\omega$ around the point $\omega = g/c$, $\vec{k} = (g/c)^{1/2}\vec{c}/c$, which satisfies the dispersion relationship, the rate of energy dissipation D is distributed in the frequency-wavenumber space along $\omega = (c^2/c_1)k_1 = (c^2/c_2)k_2$.

2.3.1. Spectrum of energy dissipation. To simplify the problem, first a case is considered in which all waves run in the same direction, and the fraction of wave crests carrying breakers is small ($\epsilon = 2\pi/gcN(\vec{c})d\vec{c} \ll 1$). As the spatial scale of a single breaker is comparable with a half of its wavelength [*Duncan*, 1981], it is reasonable to assume that the dissipation spectrum $Diss(\omega, k)$ has the shape of a white noise spectrum distributed along the line $\omega = ck$ over an area A,

$$A = dc \int_{k_1}^{k_2} k dk = \frac{1}{2} g^2 c^{-4} dc, \tag{23}$$

where the limits of integration are $k_1 = \epsilon k_2$ and $k_2 = g/c^2$. The spectral rate of energy dissipation follows from (22) and (23)

$$Diss(\omega, k) = DA^{-1} = 4\pi b g^{-3} (\frac{\omega}{k})^8 N(c), \tag{24}$$

where $\omega = ck$ (c is given), and the spectrum $Diss(\omega, k)$ is restricted along the k axis to the interval $\epsilon g/c^2 < k < g/c^2$.

Equation (24) describes the frequency-wavenumber spectral rate of energy dissipation by a narrowband of breaking waves with velocities in the range c to $c + dc$. If we consider the sea surface as a superposition of waves in a wide range of wavenumbers, the wavenumber spectrum of energy dissipation $\mathcal{D}(k)$ will be found from (24) by integration over all frequencies for a given k

$$\mathcal{D}(k) = \int Diss(\omega, k) d\omega. \tag{25}$$

Anticipating that $(\omega/k)^2 g^{-1} N(c)$ is a slowly varying function of frequency, we can extract this term out from the integral. After the integration, (25) takes the form

$$\mathcal{D}(k) = \frac{4}{7} \pi b g^{3/2} k^{-7/2} N(c). \tag{26}$$

This spectrum of the energy dissipation is obtained for unidirectional waves. The angular spreading of the energy loss due to wave breaking is defined by the number of breakers propagating in the direction range θ to $\theta + d\theta$. The directional spectrum of the energy dissipation obviously follows from (26),

$$\mathcal{D}(k, \theta) = \frac{4}{7} \pi b g^{3/2} k^{-9/2} N(c, \theta). \tag{27}$$

$N(c, \theta)$ is the two-dimensional density of frequency of wave breaking events, so that $N(c, \theta) dc d\theta$ is the expected number of breakers passing a given point per unit time in the range of speed c to $c + dc$, and in the range of direction θ to $\theta + d\theta$. Note that $N(c) = \int N(c, \theta) d\theta$.

To obtain the final equation for the spectral rate of dissipation, an explicit expression for $N(c, \theta)$ should be found. For the sake of simplicity, we will assume that the frequency of wave breaking events depends on the ratio of the saturation spectrum to some threshold level α_g,

$$2\pi \frac{c}{\omega} N(c, \theta) = \left(\frac{k^4 F(k, \theta)}{\alpha_g} \right)^{n_g + 1}, \tag{28}$$

where the parameters n_g and α_g are to be defined. Wave breaking is intensified when the local degree of saturation approaches a given threshold level. Substituting (28) into (27) we finally obtain

$$\mathcal{D}(k, \theta) = g^{3/2} k^{-7/2} \left(\frac{B(k, \theta)}{\alpha_g} \right)^{n_g} B(k, \theta). \tag{29}$$

The term $2b/(7\alpha_g) \sim 1$ is accounted for in the threshold level α_g. With $n_g = 2$, (29) corresponds to the rate of dissipation obtained by *Phillips* [1985]. For arbitrary n_g, this equation corresponds to the parameterization of the dissipation proposed by *Donelan and Pierson* [1987].

Note that in the gravity range of the wave spectrum, where dissipation is due to wave breakings, the parameters n_g and α_g are universal constants. For very short gravity waves (wavelengths less than 10-15 cm), dissipation is associated with the generation of parasitic capillaries, as described in section 2.2. If we assume that the spectral rate of dissipation of these waves is described by (29), then the parameters n_g and α_g should be functions of the dimensionless wavenumber (k/k_c).

2.3.2. Influence of the drift current on dissipation. Just beneath the surface the molecular diffusion dominates the vertical momentum flux in the water. This results in a strong shear of the drift current q_0 across a thin viscous sublayer of thickness δ. Below δ the turbulent mixing becomes important, and the vertical shear of the current is rapidly reduced. The viscous sublayer thickness δ and the shear of the drift current q_0 are defined by the relationships [e.g., *Monin and Yaglom*, 1971]

$$\delta = c_1 \frac{\nu_w}{v_*}, \tag{30}$$

$$q_0 = c_1 v_*, \tag{31}$$

where $c_1 \sim 5 - 10$ is an empirical constant, ν_w is the molecular viscosity of the water, $v_* = (\tau_s/\rho_w)^{1/2}$ is the friction velocity in the water, and τ_s is the surface stress.

Banner and Phillips [1974] showed that this current shear affects the incipient breaking of small-scale waves, thus reducing the upper limit of the wave steepness $(ak)_{max}$

$$(ak)_{max} = \frac{1}{2}(1 - \frac{q_0}{c})^2. \tag{32}$$

According to relation (32), the maximum reduction of the wave steepness occurs when $k \to k_c$. *Smith* [1990] further pointed out that wave breaking is affected by the effective shear of the drift current, defined as the difference between the surface current velocity q_0 and the velocity with which the waves are advected by the current

$$q = \frac{q_0}{1 + 2k\delta}. \tag{33}$$

Since the drift affects the wave breaking, it should be accounted for in the dissipation term (29). As proposed, the threshold level parameter α_g, which appears in (29), imposes a limit to the saturation spectrum. Dissipation due to the drift current can then be accounted for by modifying the threshold level parameter α_g,

$$\alpha_g = \alpha_{g0} \left(1 - \frac{q}{c} \cos\theta\right)^4, \tag{34}$$

where α_{g0} is the value of α_g when the drift current is zero. The cosine factor in (34) accounts for the fact that only the projection of the drift current vector (which coincides with the wind direction) on the wavenumber vector affects breaking of a wave component.

In part 1 of this paper it is shown that the surface turbulent stress is only a fraction of the total stress $\rho_a u_*^2$ at the sea surface, that is, $\tau_s = \rho_a(1 - \alpha_c)u_*^2$, where α_c is the coupling parameter. Then the effective shear of the current (33) becomes

$$q = c_1 \left[\frac{\rho_a}{\rho_w}(1 - \alpha_c)\right]^{1/2} \frac{u_*}{1 + 2\delta k}, \tag{35}$$

$$\delta = c_1 \left[\frac{\rho_a}{\rho_w}(1 - \alpha_c)\right]^{-1/2} \frac{\nu_w}{u_*}. \tag{36}$$

Thus the influence of the drift current on the rate of energy dissipation $\mathcal{D}(k, \theta)$ is introduced via modification of the threshold level parameter α_g (relations (34), (35), and (36)).

2.4. Resonant Wave-Wave Interactions

Resonant wave-wave interactions redistribute spectral wave energy in the $\vec{k}$ space. *Valenzuela and Laing* [1972] have studied in detail the three wave-wave resonant interactions in the capillary-gravity interval. They showed that the three wave-wave interactions redistribute energy from the vicinity of the wavenumber $k = k_c$ toward gravity and capillary waves. They suggested that this mechanism is responsible for the existence of the spectral gap at $k \sim k_c$, which was revealed experimentally.

The exact expression for the resonant energy spectral flux divergence is given by *Valenzuela and Laing* [1972]. In the present paper a parameterization of the three wave-wave interactions is used

$$\nabla \cdot \vec{T} \sim k^5 \omega^{-1} E^2(k, \theta) = k^{-5} \omega^3 B^2(k, \theta). \tag{37}$$

This parameterization follows from dimensional analysis and the fact that resonant three wave-wave interactions are quadratic in energy. In principle, (37) is not correct, because the three wave-wave interactions are not local in the wavenumber space. Nevertheless, (37) describes phenomenologically the resonant three wave-wave interactions, and will be used further in our model to introduce the nonlinear limitation of the wave growth in the vicinity of $k \sim k_c$.

In the gravity interval of the wave spectrum, far from the spectral peak, the four wave-wave interactions are local in the wavenumber space and the spectral flux divergence can be written as [*Phillips*, 1985]

$$\nabla \cdot \vec{T} \sim -k^{-5} \omega^3 B^3(k, \theta). \tag{38}$$

3. Spectrum of Short Wind Waves

An explicit expression for the stationary spectrum of the short wind waves results from the balance $Q = 0$ in (4). All terms of this equation were considered in section 2, where they were presented as a function of the energy (or the saturation) spectrum.

3.1. Capillary-Gravity Wave Spectrum

In the capillary-gravity range $k > k_c$ the wave spectrum can be obtained from the balance of wind input (6), viscous dissipation, generation of parasitic capillaries (16), and three wave-wave resonant interactions (37),

$$\beta_\nu \omega E(k, \theta) + \left(\frac{k_c}{k}\right)^4 \mathcal{D}(K, \theta)\mathcal{F} - \frac{k^5 E^2(k, \theta)}{\alpha_{cg}\omega} = 0. \tag{39}$$

Here $\beta_\nu = \beta\rho_a/\rho_w - 4\nu k^2/\omega$ is the difference between the growth rate and the rate of viscous dissipation, $\mathcal{D}(K,\theta)$ is the energy dissipation of the SGWs, $\mathcal{F}$ is a filter function which restricts a region in k space where the energy dissipation occurs due to the generation of parasitic capillaries, and α_{cg} is a constant to be defined. The function $\mathcal{F}$ should be close to 1 in the range ~ 60 rad m$^{-1} < K < 1/2k_c$ and decrease rapidly outside this range. We specify a mapping of this function into the capillary interval as

$$\mathcal{F}(k/k_c) = \exp(-4\left(\frac{k_c}{k}\right)^4) \tag{40}$$

for $k < 2000$ rad m^{-1} and zero for $k > 2000$ rad m^{-1}. It follows from the energy balance (39) that in the vicinity of the wavenumber $k = k_c$ the three wave-wave interactions are the only energy sink which provides the limitation of wind wave growth. Well inside the capillary range that is the molecular viscosity which provides the dissipation of energy transferred from the short gravity interval by the nonlinear cascade mechanism described in section 2.2.

The solution of (39) is

$$B(k,\theta) = \frac{\alpha_{cg}}{2}\left[\beta_\nu + \left(\beta_\nu^2 + \frac{4\tilde{\mathcal{D}}(K,\theta)\mathcal{F}(k/k_c)}{\alpha_{cg}}\right)^{1/2}\right], \tag{41}$$

where $\tilde{\mathcal{D}} = K^{7/2}g^{-3/2}\mathcal{D}$ is the dimensionless dissipation spectrum.

3.2. Short Gravity Wave Spectrum

The spectrum of short gravity waves ($k < k_c$) results from the balance of wind input (6), energy dissipation due to small-scale wave breaking (and generation of the parasitic capillaries) (29), and resonant four wave-wave interactions (38),

$$\beta_\nu \omega E(k,\theta) - \frac{g^{3/2}}{k^{7/2}} B(k,\theta)\left[\frac{B(k,\theta)}{\alpha_g}\right]^{n_g} - \nabla\cdot\vec{T} = 0. \tag{42}$$

The role of each term in the energy balance equation (42) is still not clear. *Donelan and Pierson* [1987] assumed that in the short gravity range of the wave spectrum wind input and dissipation are the dominant processes, and resonant interactions play only a minor role. *Zakharov and Zaslavskii* [1982] and *Kitaigorodskii* [1983] suggested that in the gravity range the dominant process is the resonant wave-wave interactions, and the wave spectrum results from the constant nonlinear energy flux toward the high wavenumbers. *Phillips* [1985] proposed an energy balance where all three terms in (42) are proportional to each other. This immediately gives (if $\nabla\cdot\vec{T}$ is parameterized by (38)) that the parameter n_g in the dissipation spectrum equals

$$n_g = 2. \tag{43}$$

Using this assumption, *Phillips* [1985] obtained a wave spectrum that coincides with the one proposed by *Zakharov and Zaslavskii* [1982] and *Kitaigorodskii* [1983]. The whitecap coverage of the sea calculated from this spectrum appeared to be consistent with measurements by, for example, *Monahan and Muircheartaigh* [1980]. This result is important for the present study as it implicitly confirms the proper choice of $n_g = 2$ in the dissipation term. This value of n_g is used further in our model.

Following *Donelan and Pierson* [1987], we shall assume that the energy input from the wind and the energy dissipation due to wave breaking are dominant in the short waves gravity interval. Then the saturation spectrum takes the form

$$B(k,\theta) = \alpha_g\left[\beta_\nu(k,\theta)\right]^{1/2}. \tag{44}$$

Note that in this case the sea surface variance spectrum is proportional to $u_* g^{1/2} k^{-7/2}$. As was shown by, for example, *Zakharov and Zaslavskii* [1982], this spectrum provides a constant nonlinear energy flux toward the high wavenumbers. It means that the divergence of the nonlinear energy flux has vanished, and this may justify why the nonlinear interactions (the third term in the energy balance (42)) can be omitted.

3.3. Generalized Spectrum

To patch the capillary-gravity spectrum (41) and the gravity spectrum (44) in the vicinity of the wavenumber $k = k_c$, we define the shape of the generalized short wind waves spectrum $B_s(k,\theta)$ as

$$B_s(k,\theta) = \alpha\left\{\frac{1}{2}\left[\beta_\nu(k,\theta) + \mathcal{A}^{1/2}\right]\right\}^{1/n}, \tag{45}$$

$$\mathcal{A} = \left(\beta_\nu^2(k,\theta) + 4\frac{\beta_\nu(K,\theta)}{\alpha}B_s(K,\theta)\mathcal{F}(k/k_c)\right), \tag{46}$$

where the parameters α and n are

$$\alpha = \alpha_0(1 - \frac{q}{c}\cos\theta)^4, \tag{47}$$

$$\ln(\alpha_0) = (\ln(\alpha_{cg}) - \ln(\alpha_{g0}))\phi(k/k_c) + \ln(\alpha_{g0}), \tag{48}$$

$$n^{-1} = \frac{1}{2}\phi(k/k_g) + \frac{1}{2}. \tag{49}$$

In (48) α_{g0} and α_{cg} are constants defining the threshold level (without the influence of drift current) in the gravity range and in the vicinity of $k = k_c$, respectively. Relation (47) (where q is defined by (35) with a mean value $c_1 = 7$) accounts for the influence of the drift current on the threshold level. Formally, the function $\phi(k/k_c)$ in (48) and (49) provides the patching of the capillary-gravity and gravity intervals. Its physical significance is that $\phi(k/k_c)$ describes the transition be-

tween the regimes where the energy loss is dominated by wave breaking, by generation of parasitic capillaries, and by resonant three wave-wave interactions, respectively. This function is specified as

$$\phi(k/k_c) = \min[(k/k_c), 1]. \quad (50)$$

To complete the model, the last two constants α_{g0} and α_{cg} are to be defined. The former constant provides patching of the short gravity wave spectrum with the energy containing part of the *Donelan et al.* [1985] spectrum with correction of *Elfouhaily et al.* [1997]. This constant is chosen to be $\alpha_{g0} = 0.03$. The latter constant α_{cg} is defined (see section 4.1) after the comparison between the model spectrum and measurements [*Jähne and Riemer*, 1990; *Hara et al.*, 1997] at $k \simeq k_c$. It will be shown that fitting the model to measurements gives $\alpha_{cg} = 0.09$.

3.4. Coupling With the Atmospheric Boundary Layer

The coupling between the surface waves and the air boundary layer is realized via the resistance law

$$C_D^{1/2} = \frac{u_*}{u_{10}} = \kappa \left(\int_{z_0^\nu}^{10} [1 - \alpha_c f(z)]^{3/4} \, d(\ln z) \right)^{-1} \quad (51)$$

obtained in part 1. In (51), u_{10} is the wind speed at 10 m height, z_0^ν is the viscous roughness scale (equation (3) in part 1), $f(z)$ is a dimensionless function describing the vertical distribution of the mean wave-induced stress (equation (24) in part 1), and α_c is the coupling parameter

$$\alpha_c = \frac{\tau^w(0)}{u_*^2}. \quad (52)$$

The wave-induced stress at the surface (the form drag) $\tau^w(0)$ is calculated from the saturation spectrum (45) and the growth rate parameter β (5),

$$\tau^w(0) = \int_0^\infty \int_{-\pi}^{\pi} c^2 B_s(k,\theta) \beta(k,\theta) \cos\theta \, d\theta \, d(\ln k). \quad (53)$$

Equations (45)-(53) describe self-consistently the short wave spectrum and the atmospheric boundary layer.

Energy containing long waves in the peak of the wave spectrum support a part ($\sim 10\% - 20\%$) of the momentum flux to the sea surface [*Makin and Kudryavtsev*, this issue], and thus influence the balance of short wind waves. To account for that fact a long wave spectrum should be added to the described model of the short wave spectrum. Therefore the long wave spectrum model proposed by *Donelan et al.* [1985] with corrections made by *Elfouhaily et al.* [1997] is chosen. The final model of the wave spectrum in the full wavenumber range (from the spectral peak to capillaries) is presented as a sum of the long wave spectrum $B_l(u_{10}/c_p, k, \theta)$ and the short wind wave spectrum (45)

$$B(k,\theta) = B_l(u_{10}/c_p, k, \theta) + B_s(k,\theta), \quad (54)$$

where u_{10}/c_p is the inverse wave age, and c_p is the phase velocity in the peak of the spectrum.

4. Results

4.1. Spectral Characteristics

Figures 1 and 2 show the model saturation spectrum and laboratory measurements of the up-wind $B(k,0)$ and the omnidirectional $B(k)$ saturation spectrum at wavelengths $\lambda = 0.008$ m ($k = 785$ rad m^{-1}), $\lambda = 0.016$ m ($k = 393$ rad m^{-1}), $\lambda = 0.031$ m ($k = 203$ rad m^{-1}), and $\lambda = 0.063$ m ($k = 100$ rad m^{-1}), reported by *Jähne and Riemer* [1990] and *Hara et al.* [1997]. Model calculations have been done for the fetches, where laboratory measurements were obtained (100 m [*Jähne and Riemer*, 1990] and 13 m [*Hara et al.*, 1997]). However, only one model line is shown in the figures, as model results for both fetches are very close. That is explained by the fact that our short wave spectrum has no direct dependence on the fetch or wave age. The measured values of the saturation level at $\lambda = 0.016$ m were used to adjust α_{cg} to 0.09. Then, overall a good agreement is obtained for $\lambda = 0.008$ m, a wave component which corresponds to the parasitic capillary range. The capillary wave spectrum (45), $k > 2k_c$, does not require any adjustments and directly results from the short gravity wave spectrum. This fact actually justifies that generation of parasitic capillaries indeed plays the dominant role in the balance equation of capillary waves. In the gravity range ($\lambda = 0.031$ m and $\lambda = 0.063$ m) the comparison is reasonable for the lowest values of the friction velocity. At large values the measured spectrum exceeds the model one.

The up-wind and omnidirectional spectra of a developed sea ($u_{10}/c_p = 0.83$) at various wind speeds are shown in Figure 3. At low winds there is a spectral gap in the vicinity of $k = k_c$, which is filled up with an increase of the wind speed. Such a peculiarity in the spectral form was observed in the laboratory experiments of *Cox* [1958] and *Zhang* [1995]. This spectral gap at low winds is caused by the viscous dissipation, which increases toward the higher wavenumbers. The gap occurs at wavenumbers up to $k \sim 2k_c$. At higher wavenumbers the generation of parasitic capillaries takes place which overcomes the viscous dissipation. A local spectral peak is formed in the vicinity of $k = 1000$ rad m^{-1}, moving to $k = 700$ rad m^{-1} with increasing wind speed. In the capillary range the saturation spectrum rapidly drops toward the higher wavenumbers, which is again consistent with measurements [*Jähne and Riemer*, 1990; *Zhang*, 1995].

Figure 4 illustrates the influence of the shear of the drift current inside the viscous sublayer on the saturation spectrum. When this mechanism is taken into account, the spectral level is suppressed. The effect is most pronounced in the vicinity of $k \sim 100$ rad m^{-1}.

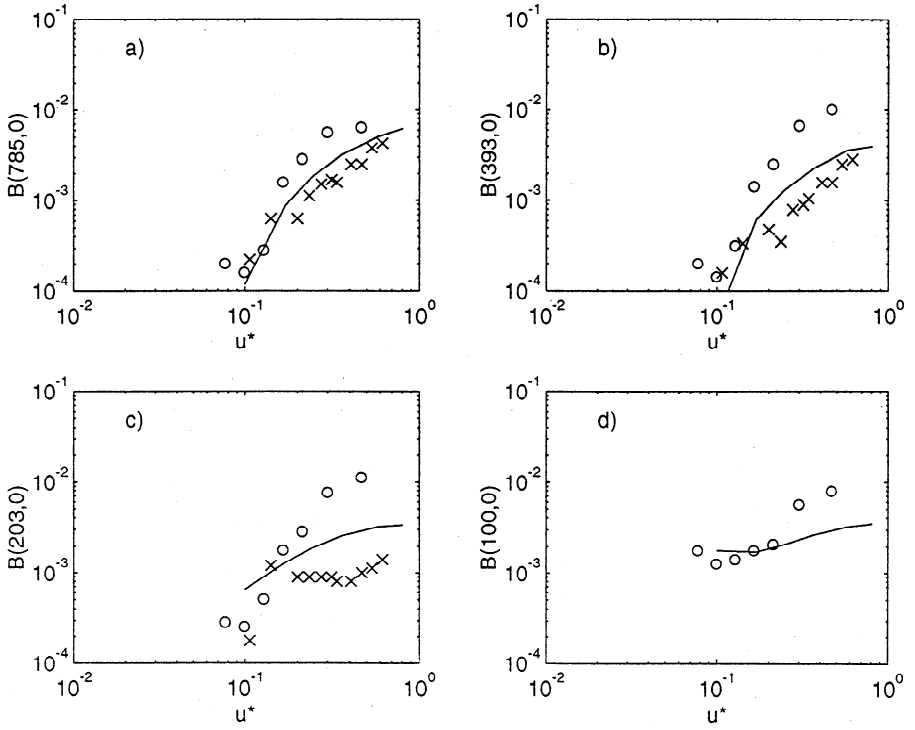

Figure 1. Up-cross section of the saturation spectrum $B(k,0)$ versus the friction velocity u_* in meters. Solid line, model results; circles, measurements of *Jähne and Riemer* [1990]; crosses, measurements of *Hara et al.* [1997].

At a wind speed of 20 $\mathrm{m\,s^{-1}}$ the drift current reduces the spectrum level by 4 times.

The angular spectrum distributions $B(k,\theta)/B(k,0)$ at $\lambda = 0.008$ m ($k = 785$ $\mathrm{rad\,m^{-1}}$), $\lambda = 0.016$ m ($k = 393$ $\mathrm{rad\,m^{-1}}$), $\lambda = 0.031$ m ($k = 203$ $\mathrm{rad\,m^{-1}}$), and $\lambda = 0.063$ m ($k = 100$ $\mathrm{rad\,m^{-1}}$) are shown in Figure 5. It appears that the angular width decreases with increasing the wavenumber, and at $k > k_c$ it remains

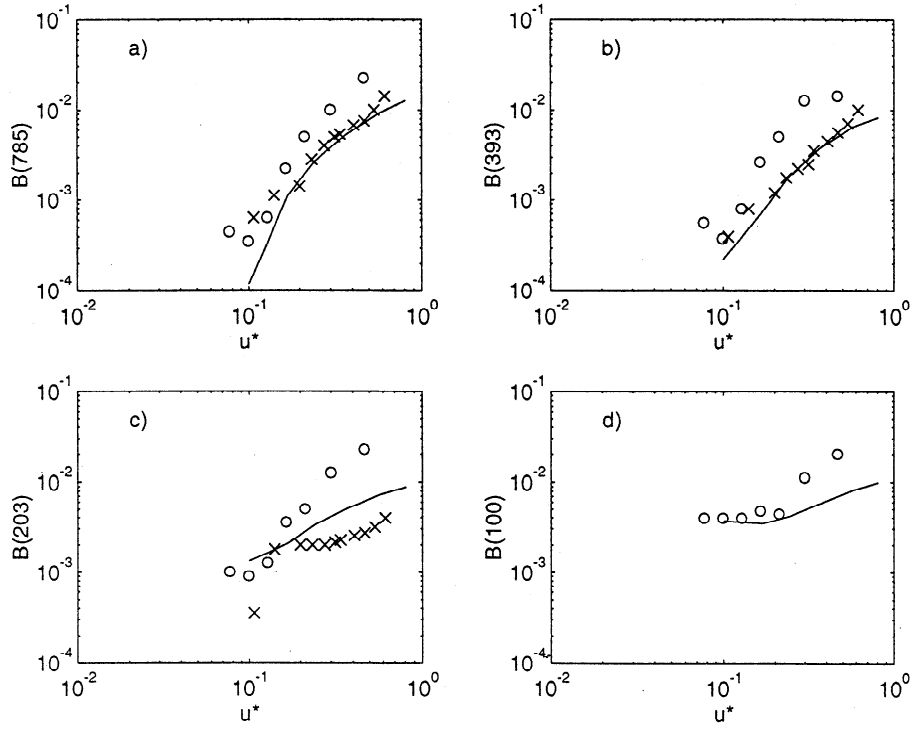

Figure 2. The same as in Figure 1 but for omnidirectional saturation spectrum $B(k)$.

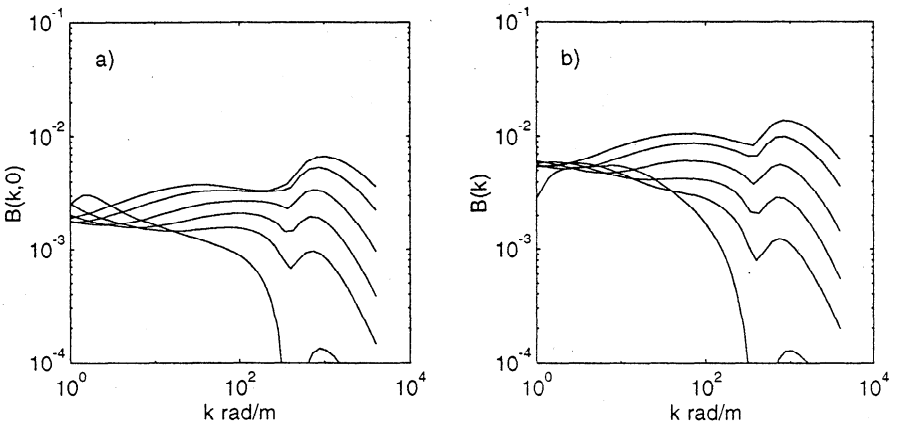

Figure 3. (a) Up-cross section of the saturation spectrum $B(k,0)$ versus the wavenumber k for different wind speeds u_{10}. Curves from the bottom to the top: 3, 5, 7, 10, 15, and 20 $\mathrm{m\,s^{-1}}$. (b) The same as in Figure 3a but for omnidirectional saturation spectrum $B(k)$.

approximately constant. The wave energy in this range is mainly supplied by the generation of parasitic capillaries, and the angular spreading is then proportional to an angular spreading associated with the growth rate parameter of carrying gravity waves. The narrowing of the capillary-gravity angular width was revealed in the laboratory experiment of *Zhang* [1995] and mentioned by *Banner et al.* [1989]. This effect is parameterized in the empirical spectra proposed by *Fung and Lee* [1982] and *Elfouhaily et al.* [1997].

The second remarkable feature of the capillary-gravity wave energy angular spreading is its widening with increasing wind speed. This effect directly results from the impact of the drift current. As follows from (34) and (45), wave components which propagate along the wind direction are damped most. For waves propagating at relatively large angles the effect is small.

4.2. Integral Characteristics of the Spectrum

4.2.1. Surface mean squared slope. The mean squared slope of the sea surface is mainly supported by the short wind waves, hence this integral parameter can be used to check the model consistency. The model

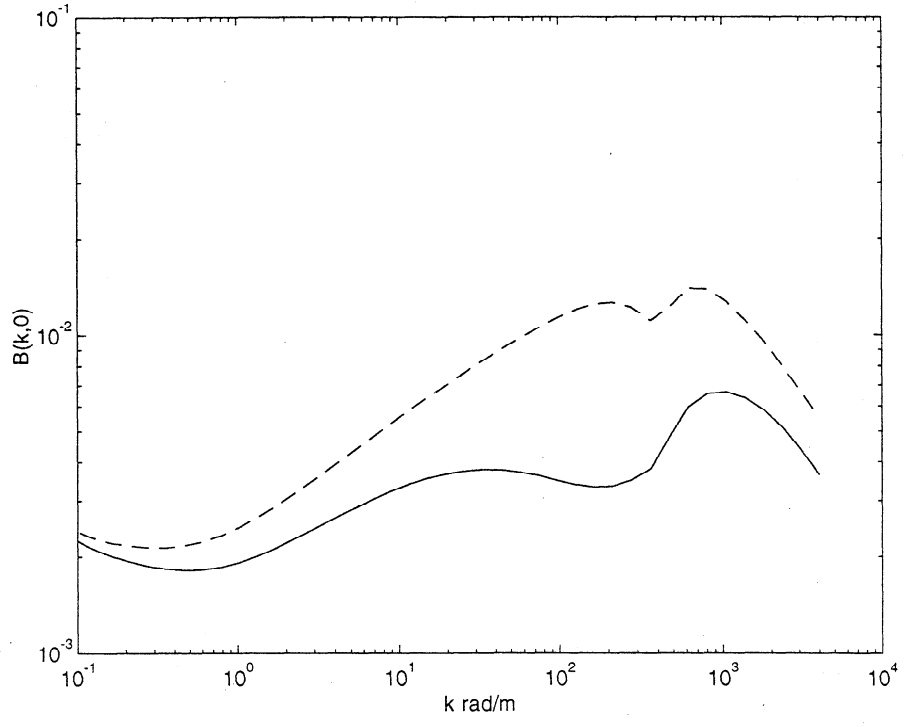

Figure 4. Up-cross section of the saturation spectrum $B(k,0)$ versus the wavenumber k for the wind speed $u_{10} = 20\ \mathrm{m\,s^{-1}}$. Solid line, surface current shift is accounted for (equation (34)); dashed line, surface current shift is not accounted for.

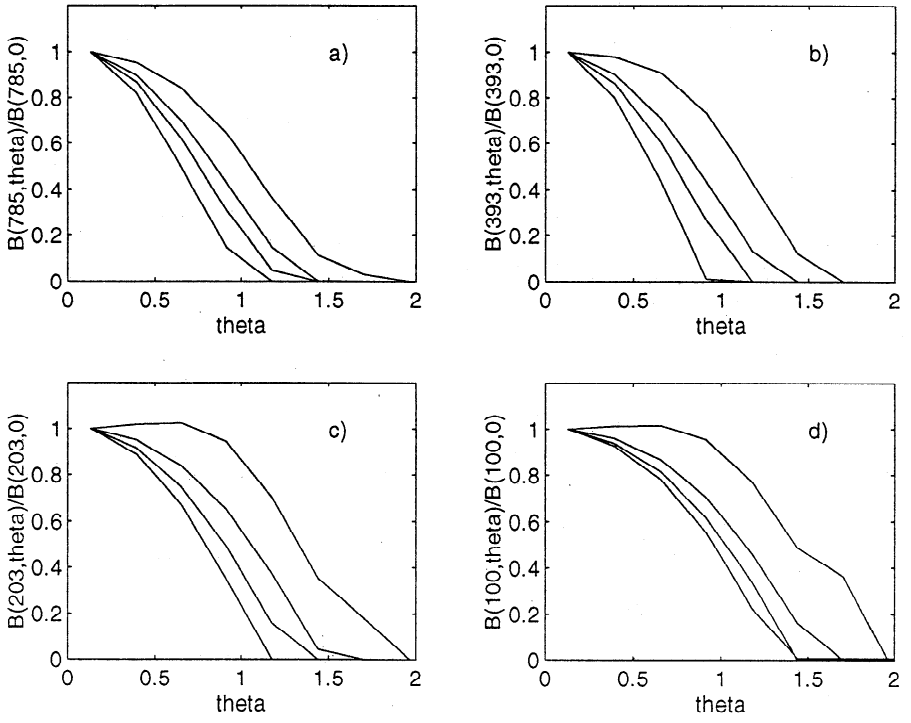

Figure 5. Angular distribution $B(k,\theta)/B(k,0)$ for different wind speeds u_{10}. Angle θ is in rad. Curves from the bottom to the top: 5, 7, 10, and 20 m s^{-1}. (a) Variable $k = 785$ rad m^{-1}, (b) $k = 393$ rad m^{-1}, (c) $k = 203$ rad m^{-1}, and (d) $k = 100$ rad m^{-1}.

estimates of the up-wind $< \zeta_x^2 >$ and the cross-wind $< \zeta_y^2 >$ mean squared slopes are

$$< \zeta_x^2 >= \int \cos^2(\theta) B(k,\theta) d\theta d(\ln(k)), \quad (55)$$

$$< \zeta_y^2 >= \int \sin^2(\theta) B(k,\theta) d\theta d(\ln(k)). \quad (56)$$

respectively. The total mean squared slope ζ_0 is

$$\zeta_0 =< \zeta_x^2 > + < \zeta_y^2 > . \quad (57)$$

Figure 6 gives model and measured [*Cox and Munk*, 1954] mean squared slopes as a function of the wind speed (the reanalysis of the *Cox and Munk* [1954] data done by *Wu* [1990] is also shown). Overall, a good agreement is obtained.

The ratio $< \zeta_y^2 > / < \zeta_x^2 >$ is an integral measure of the spectrum angular anisotropy. This ratio versus the wind speed is given in Figure 6 along with the observation of *Cox and Munk* [1954]. Neither model calculations nor field observation demonstrate any systematic trend in dependence of $< \zeta_y^2 > / < \zeta_x^2 >$ on wind

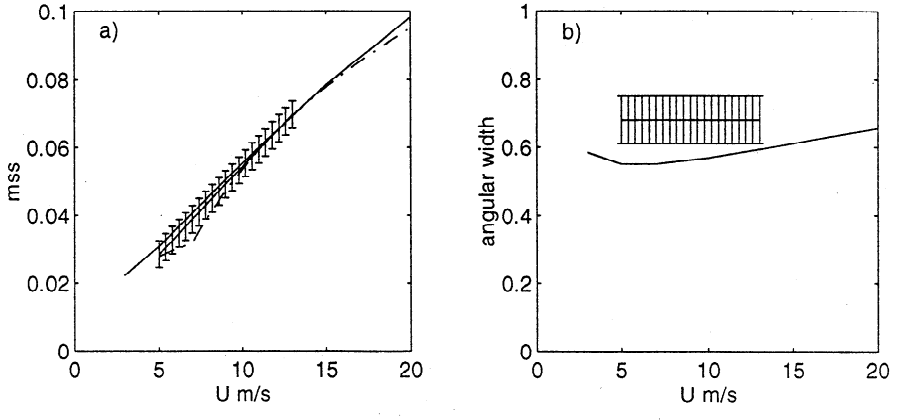

Figure 6. (a) The mean square slope ζ_0 versus the wind speed u_{10}. Solid curve, model results; solid line with bars, regression line of *Cox and Munk* [1954], dashed-dotted line, regression line of *Wu* [1990]. (b) Ratio $< \zeta_y^2 > / < \zeta_x^2 >$ versus the wind speed u_{10}. Solid curve, model results; solid line with bars, regression of *Cox and Munk* [1954].

speed. The averaged value 0.68 reported by *Cox and Munk* [1954] exceeds slightly the model estimate.

4.2.2. Skewness of the sea surface slopes. In their experiment, *Cox and Munk* [1954] also reported skewness measurements of the surface slopes. The skewness was defined by a shift from the specular direction of the brightest point in the Sun glitter. *Longuet-Higgins* [1982] analyzed different mechanisms that could contribute to the skewness, and concluded that the most probable one is the modulation of short wind waves by longer waves. The simple sea surface model adopted by *Longuet-Higgins* [1982] consists of a sum of a long wave and a short wave modulated by the long wave

$$\zeta_x = AK\sin\phi + [ak + \delta(ak)\cos(\phi - \gamma)]\sin\phi', \quad (58)$$

where ζ_x is the up-wind slope of the wave surface, AK and ak are the steepness of the long and the short wave, respectively, ϕ and ϕ' are their phase functions, $\delta(ak)$ is the amplitude of the short wave steepness modulation, and γ is the phase of the modulation. Such a two-scale model gives

$$< \zeta_x^3 >= \frac{3}{2}AK(ak\delta(ak))\sin\gamma. \quad (59)$$

According to the present development, parasitic capillaries are spread on the forward face of short gravity waves and attenuate due to viscous dissipation. Hence we can take $\sin\gamma = 1$ and $\delta(ak) = ak$. Since wind input is negligible in the generation of parasitic capillaries (see section 2.2.3), the model skewness is defined as

$$< \zeta_x^3 >= 3\sqrt{2}\left[\int_{k_1}^{k_c/2} B(k,\theta)\cos^2 d\theta d(\ln k)\right]^{1/2} \times \times \int_{k>2k_c} B(k,\theta)\cos^2\theta d\theta d(\ln k) \quad (60)$$

where $k_1 = 2\pi/0.15$ rad m^{-1} is the wavenumber restricting the interval of short gravity waves which generate parasitic capillaries. The skewness coefficient

$$\lambda_3 = \frac{< \zeta_x^3 >}{< \zeta_x^2 >^{3/2}} \quad (61)$$

is shown in Figure 7. The values of λ_3 as calculated by *Longuet-Higgins* [1982] from *Cox and Munk*'s [1954] data are also presented. The model skewness values related to parasitic capillaries are comparable with the observed ones which indicates their dominant influence on the slope skewness measurements.

4.3. Interaction Between Wind and Waves

The coupled sea surface–atmosphere model should reproduce in the first place the known wind speed dependency of the drag coefficient C_D. In Figure 8a the model results are shown together with the parametrization of the drag coefficient obtained in the open ocean [*Anderson*, 1993; *Donelan and Pierson*, 1987; *Large and Pond*, 1982; *Smith*, 1980]. Given a typical error in stress measurements of about 15%-20% [*Donelan*, 1990], the model results compare well with the observations (see also Figure 3 in part 1).

The sea surface drag is supported by the viscous stress and the wave-induced stress. In part 1 we show the dominant role of the form drag, expressed in terms of the coupling parameter $\alpha_c = \tau^w(0)/u_*^2$, in the coupling between wind and waves. The wind speed dependency of α_c is shown in Figure 8b for the proposed wave spectrum. Recent direct measurements of the coupling parameter were obtained in the laboratory experiments by *Banner and Peirson* [1998]. They found that the coupling parameter is equal to 0.38 for 7 m s^{-1} and to 0.67 or less for 13 m s^{-1}. These experimental estimates are shown in Figure 8b, and are in a good agreement with model calculations.

To further assess which waves contribute most to the wave-induced stress at the surface, the surface flux spectrum and the cumulative spectrum are presented in Figures 8c and 8d. The omnidirectional spectrum of the momentum flux to waves $T^w(k)$ is defined as

$$T^w(k) = \int_{\pi}^{\pi} \beta c^2 \cos\theta B(k,\theta)d\theta, \quad (62)$$

so that

$$\tau^w(0) = \int_0^{\infty} T^w(k)d(\ln k). \quad (63)$$

The cumulative spectrum is

$$Cu(k) = \frac{1}{\tau_0^w}\int_k^{\infty} T^w(k)d(\ln k). \quad (64)$$

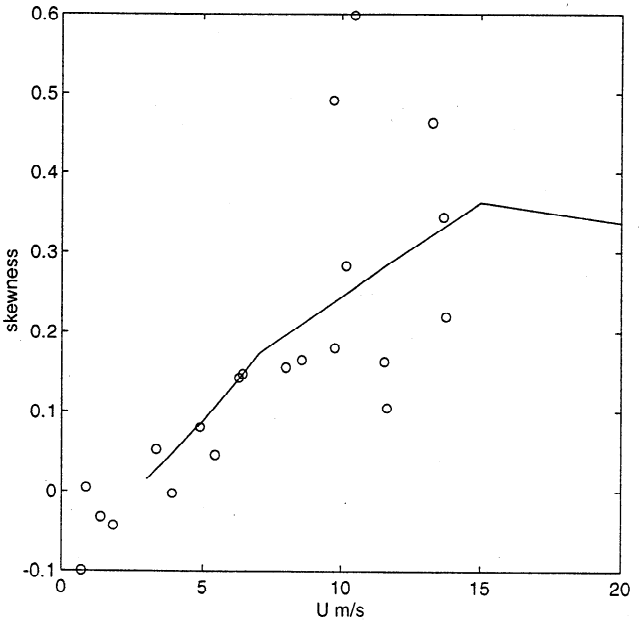

Figure 7. The skewness coefficient, (61), versus the wind speed u_{10}. Solid curve, model results; circles, analysis by *Longuet-Higgins* [1982] based on data of *Cox and Munk* [1954].

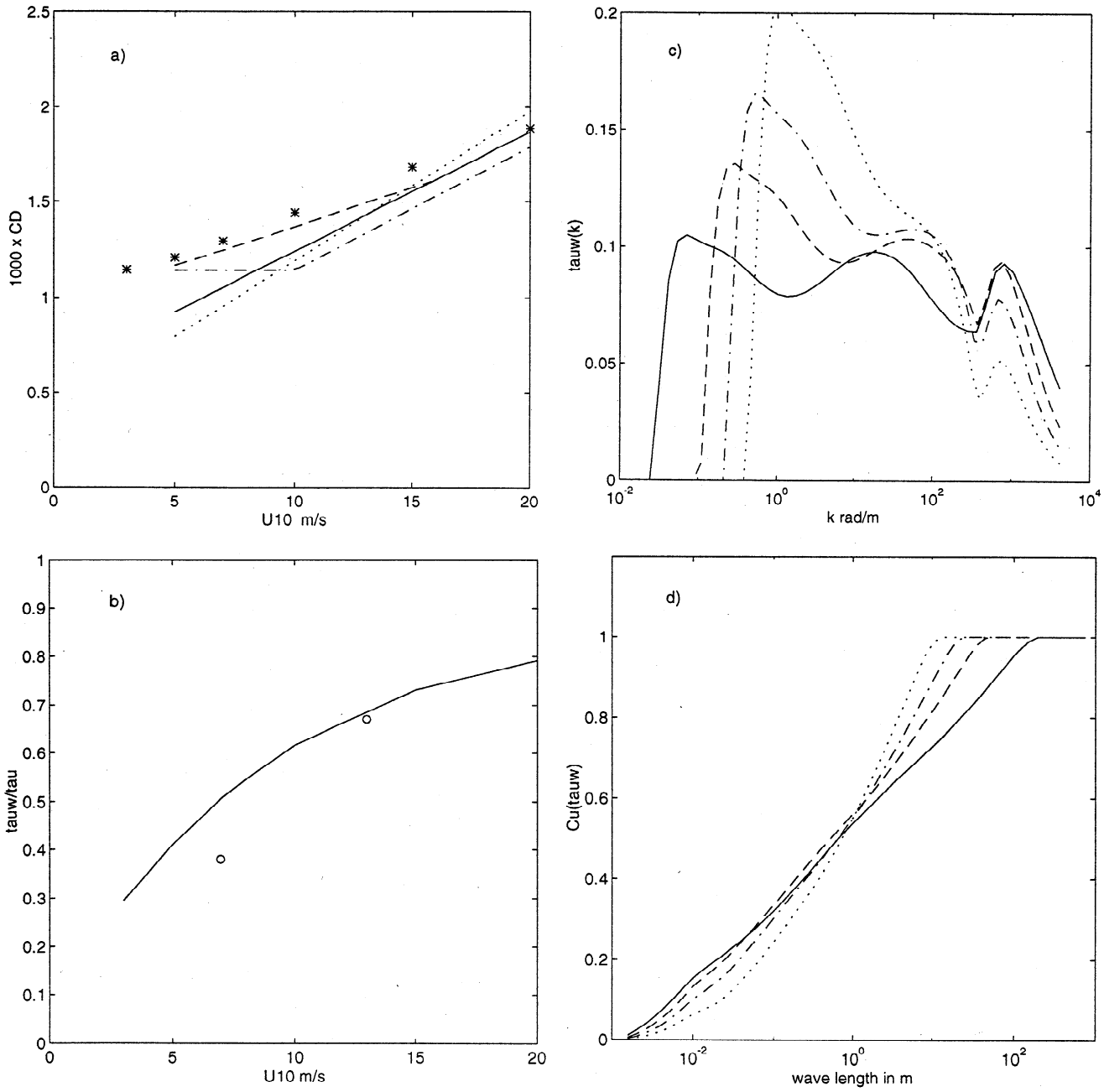

Figure 8. (a) Drag coefficient versus u_{10}. Stars, model results; solid line, regression line from *Smith* [1980]; dashed line, regression line from *Donelan and Pierson* [1987]; dashed-dotted line, regression line from *Large and Pond* [1982]; dotted line, regression line from *Anderson* [1993]. (b) Coupling parameter $\tau^w(0)/u_*^2$. Solid line, model results; circles, experiment of *Banner and Peirson* [1998]. (c) Spectrum and (d) cumulative spectrum of the wave-induced stress at the sea surface. Wind speed: solid line, $u_{10} = 20\ \mathrm{m\,s^{-1}}$; dashed line, $10\ \mathrm{m\,s^{-1}}$; dashed-dotted line, $7\ \mathrm{m\,s^{-1}}$; dotted line, $5\ \mathrm{m\,s^{-1}}$.

The latter is shown as a function of the wavelength $\lambda = 2\pi/k$, and an increase of the wave-induced stress is found when more and more longer waves are taken into account in the integral (64).

The spectral distribution of $T^w(k)$ varies with the wind speed. At low winds the form drag is mainly supported by decimeter to a few meters waves. With increasing wind speed, the role of centimeter waves becomes more important. A local spectral maximum is developed in the vicinity of $k = 700 - 800\ \mathrm{rad\,m^{-1}}$ and waves between 0.001 m and 0.1 m contribute about 40% to the wave-induced stress. It is interesting to note that for all wind speeds about 60% of the wave-induced stress is supported by waves shorter than 1 m, though the spectral distribution of this flux is rather different for low and high wind speeds.

5. Summary and Conclusions

In the present paper a physical model of the short wind wave spectrum in the wavelength range from a few millimeters to a few meters is proposed. The spectrum shape results from the solution of the energy spectral density balance equation, which includes wind input, dissipation due to molecular viscosity and breaking of waves, nonlinear cascade generation of parasitic capillaries, and resonant interactions. The role of each term is different depending on what spectral interval is considered.

In the capillary range the wave spectrum is mainly determined by the generation of parasitic capillaries and by their attenuation due to molecular viscosity. It is suggested that generation of parasitic capillaries by sharp crests completely provides the energy loss of short gravity waves (with wavelengths less than 10-15 cm). In the present model this mechanism is accounted for through the spectral energy source, which describes the nonlinear cascade energy flux from the short gravity wave spectral area around the wavenumber K to the capillary wave area around the wavenumber $k = g/(\gamma K)$. The energy loss by gravity waves due to the emission of capillaries is compensated by the energy input from the wind. A balance between the nonlinear cascade source of parasitic capillaries and their viscous dissipation gives the shape of the capillary wave spectrum. This shape is shown to be consistent with measurements of *Jähne and Reimer* [1990] and *Zhang* [1995].

In the gravity interval $k < k_c = (g/\gamma)^{1/2}$ wind input and dissipation due to wave breaking play a dominant role in the energy balance. The former is parameterized through the surface turbulent stress which is the difference between the total stress and the form drag. At moderate and strong winds, waves support a significant part of the total stress, hence the parameterization of energy input from the wind through the surface turbulent stress is of primary importance.

To describe the energy loss due to wave breaking, the approach developed by *Phillips* [1985] is used. This approach is based on the experimental finding by *Duncan* [1981] that breakers of different scales are geometrically similar. Introducing the breaking events statistics, and accounting for the fact that breaking of waves is a relatively rare event, an explicit relationship for the rate of energy spectral density loss $\mathcal{D}(\vec{k},\omega)$ in $\omega - \vec{k}$ space is obtained. The two-dimensional wavenumber dissipation spectrum is defined by the integration of $\mathcal{D}(\vec{k},\omega)$ over all frequencies and is presented as a power dependence of the ratio of the saturation spectrum and some threshold level. The shear of the drift current in the water viscous sublayer affects the incipient breaking of waves and consequently the energy dissipation by wave breaking [*Banner and Phillips*, 1974]. This mechanism is taken into account through the correction of the threshold level. The shape of the short gravity waves spectrum is found from the balance of wind input and dissipation due to wave breaking. For very short gravity waves breaking results in the generation of parasitic capillaries.

To obtain the short wind wave spectrum which is valid in the full wavenumber domain (from a few millimeters to a few meters), the gravity and the capillary-gravity wave spectra are patched in the vicinity of k_c, the wavenumber corresponding to the minimum phase velocity. The resulting model reasonably reproduces the known empirical statistical properties of the sea surface. The spectral shape is consistent with data from laboratory measurements of *Jähne and Reimer* [1990], *Hara et al.* [1997], and *Zhang* [1995]. At low wind speed there is a spectral gap in the vicinity of k_c, which is filled up when the wind speed increases. In the capillary range at $k \sim 700 - 1000$ rad m^{-1} there is a local spectral peak which originates from the generation of parasitic capillaries. At higher wavenumbers the saturation spectrum drops rapidly due to viscous dissipation. The angular width of the spectrum decreases with increasing wavenumber, and at $k > k_c$ it remains approximately constant. At the same time the angular spreading of the energy spectral density grows with the wind speed, which results from the fact that the drift current suppresses waves running in the wind direction.

The model wind dependence of the total mean squared slope and the ratio of cross-wind to up-wind mean squared slope is consistent with *Cox and Munk*'s [1954] measurements. The slope skewness is the most sensitive integral parameter of the sea surface. Within the frame of our model the skewness is governed by parasitic capillaries riding on the forward face of a carrying short gravity wave. Model estimates agree reasonably well with the analysis by *Longuet-Higgins* [1982] based on *Cox and Munk*'s [1954] data.

The model also reproduces convincingly the known features of the atmospheric boundary layer, and first of all the wind speed dependence of the drag coefficient, as compared to measurements obtained in the open ocean. The model values of the coupling parameter agree well with direct laboratory measurements of *Banner and Peirson* [1998]. It is shown that waves shorter than 1 m support about one half of the wave-induced momentum flux at the surface, regardless of the wind speed. The fact that the short waves are strongly coupled to the wind dictates the use of a coupled short waves–atmospheric boundary layer model in the air-sea interaction studies.

Acknowledgments. This research was sponsored by the Office of Naval Research (ONR grant N00014-98-1-0437, N00014-98-1-0653, PR 98PR04572-00, and 98PR05889-00), by INTAS-International Association (reference INTAS 96 - 1817), and EU Environment Programme (contract ENV4-CT97-0460, ASPEN project).

References

Anderson, R.J., A study of wind stress and heat flux over the open ocean by the inertial-dissipation method, *J. Phys. Oceanogr., 23*, 2153-2161, 1993.

Apel, J.R., An improved model of the ocean surface wave vector spectrum and its effects on radar backscatter, *J. Geophys. Res., 99*, 16,269-16,290, 1994.

Banner, M.L., and W.L. Peirson, Tangential stress beneath wind-driven air-water interfaces, *J.Fluid Mech., 364*, 115-145, 1998.

Banner, M.L., and O.M. Phillips, On the incipient breaking of small scale waves, *J.Fluid Mech., 65*, 647-656, 1974.

Banner, M.L., I.S.F. Jones, and J.C. Trinder, Wavenumber spectra of short gravity waves, *J.Fluid Mech., 198*, 321-344, 1989.

Belcher, S.E., and J.C.R. Hunt, Turbulent shear flow over slowly moving waves, *J.Fluid Mech., 251*, 109-148, 1993.

Belcher, S.E., and J.C. Vassilicos, Breaking waves and the equilibrium range of wind-wave spectra, *J.Fluid Mech., 342*, 377-401, 1997.

Chang, J.H., R.N. Wagner, and C.Y. Henry, Measurements of high frequency capillary waves on steep gravity waves, *J.Fluid Mech., 83*, 401-415, 1978.

Cox, C.S., Measurements of slopes of high frequency waves, *J. Mar. Res., 16*, 199-225, 1958.

Cox, C.S., and W.H. Munk, Statistics of the sea surface derived from Sun glitter, *J. Mar. Res., 13*, 198-227, 1954.

Crapper, G.D., Non-linear capillary waves generated by steep gravity waves, *J.Fluid Mech., 40*, 149-159, 1970.

Donelan, M.A., Air-sea interaction, *Sea Ocean Eng. Sci., 9*, 239-292, 1990.

Donelan, M.A., and W.J. Pierson, Radar scattering and equilibrium ranges in wind-generated waves with applications to scatterometry, *J. Geophys. Res., 92*, 4971-5029, 1987.

Donelan, M.A., J. Hamilton, and W.H. Hui, Directional spectra of wind generated waves, *Philos. Trans. R. Soc. London, Ser. A, 315*, 509-562, 1985.

Duncan, J.H., An experimental investigation of breaking waves produced by towed hydrofoil, *Proc. R. Soc. London A, 377*, 331-348, 1981.

Elfouhaily, T., B. Chapron, K. Katsaros, and D. Vandemark, A unified directional spectrum for long and short wind-driven waves, *J. Geophys. Res., 102*, 15,781-15,796, 1997.

Fung, A.K., and K.K. Lee, A semi-empirical sea-spectrum model for scattering coefficient estimation, *IEEE J. Oceanic Eng., OE-7(4)*, 166-176, 1982.

Hara, T., E.J. Bock, and M. Donelan, Frequency- wavenumber spectrum of wind-generated gravity-capillary waves, *J. Geophys. Res., 102*, 1067-1072, 1997.

Jähne, B., and K.S. Riemer, Two-dimensional wave number spectra of small-scale water surface waves, *J. Geophys.Res., 95*, 11,531 -11,546, 1990.

Janssen, P.A.E.M., Wave-induced stress and the drag of air flow over sea waves, *J. Phys. Oceanogr., 19*, 745-754, 1989.

Kitaigorodskii, S.A., On the theory of the equilibrium range in the spectrum of wind-generated gravity waves, *J. Phys. Oceanogr., 13*, 816-827, 1983.

Kudryavtsev, V.N., A physical model of capillary-gravity wave spectrum, *Morskoi Hydrophys. J. 2*, 3-14, 1996.

Large, W.G., and S. Pond, Sensible and latent heat flux measurements over the ocean, *J. Phys. Oceanogr., 12*, 464-482, 1982.

Longuet-Higgins, M.S., The generation of capillary waves by steep gravity waves, *J. Fluid Mech., 16*, 138-159, 1963.

Longuet-Higgins, M.S., On the skewness of sea-surface slopes, *J. Phys. Oceanogr., 12*, 1283-1291, 1982.

Makin, V.K., and V.N. Kudryavtsev, Coupled sea surface–atmosphere model, 1, Wind over waves coupling, *J. Geophys. Res.*, this issue.

Makin, V.K., V.N. Kudryavtsev, and C. Mastenbroek, Drag of the sea surface, *Boundary Layer Meteorol., 73*, 159-182, 1995.

Monahan, E.C., and I. Muircheartaigh, Optimal power-law description of oceanic whitecap coverage dependence on wind speed, *J. Phys. Oceanogr., 10*, 2094-2099, 1980.

Monin, A.S., and A.M. Yaglom, *Statistical Fluid Mechanics*, 769 pp., MIT Press, Cambridge, Mass., 1971.

Phillips, O.M., *The Dynamics of the Upper Ocean*, 336 pp., Cambridge Univ. Press, New York, 1977.

Phillips, O.M., Spectral and statistical properties of the equilibrium range in the wind-generated gravity waves, *J. Fluid Mech., 156*, 505-531, 1985.

Plant, W.J., A relationship between wind stress and wave slope, *J. Geophys. Res., 87*, 1961-1967, 1982.

Ruvinsky, K.D., F.I. Feldstein, and G.I. Freidman, Numerical simulation of the quasi-stationary stage of ripple excitation by steep gravity-capillary waves, *J. Fluid Mech., 230*, 339-353, 1991.

Smith, J.A., Modulation of short wind waves by long waves, in *Surface Waves and Fluxes*, vol. 1, edited by G.L. Geernaert and W.J. Plant, 336 pp., Kluwer Acad., Norwell, Mass., 1990.

Smith, S.D., Wind stress and heat flux over the ocean in gale force winds, *J. Phys. Oceanogr., 10*, 709-726, 1980.

Toba, Y., Local balance in the air-sea boundary processes, III, On the spectrum of wind waves, *J. Ocean Soc. Jpn., 29*, 209-220, 1973.

Valenzuela, G.R., and M.B. Laing, Nonlinear energy transfer in gravity-capillary wave spectra, with applications, *J. Fluid Mech., 54*, 507-520, 1972.

Wu, J., Mean square slopes of the wind-disturbed water surface, their magnitude, directionality, and composition, *Radio Sci., 25*, 37-48, 1990.

Yermakov, S.A., K.D. Ruvinskiy, S.G. Salashin, and G.I. Freydman, Experimental investigation of the generation of capillary-gravity ripples by strongly non-linear waves on the surface of a deep fluid, *Izv. Akad. Nauk SSSR Fiz. Atmos. Oceana, 22*, 835-842, 1986.

Zakharov, V.Y., and M.M. Zaslavskii, The kinetic equation and Kolmogorov spectra in a low turbulence theory of wind waves, *Izv. Akad. Nauk SSSR Fiz. Atmos. Oceana, 18*, 747-753, 1982.

Zhang, X., Capillary-gravity and capillary waves generated in a wind wave tank: Observations and theories, *J. Fluid Mech., 289*, 51-82, 1995.

B. Chapron, Institut Français de Recherche pour l'Exploitation de la Mer, Centre de Brest, B.P. 70, 29280 Plouzané, France. (bchapron@ifremer.fr)

V. N. Kudryavtsev, Marine Hydrophysical Institute, Kapitanskaya 2, 335000 Sevastopol, Ukraine. (odmi@alpha.mhi.iuf.net)

V. K. Makin, Royal Netherlands Meteorological Institute, P.O. Box 201, 3730 AE De Bilt, Netherlands. (makin@knmi.nl)

(Received October 22, 1997; revised October 23, 1998; accepted January 4, 1999.)